Precision Engineering 42 (2015) 346–351

Contents lists available at ScienceDirect

Precision Engineering

journal homepage: www.elsevier.com/locate/precision

Technical note

Entangled structures as high cycle compression springs

Folkers E. Rojas*, Alexander H. Slocum

Department of Mechanical Engineering, Massachusetts Institute of Technology, Cambridge, MA 02139, USA

ARTICLE INFO

Article history:
Received 2 February 2015
Accepted 20 April 2015
Available online 27 May 2015

Keywords:
Entangled structures
Foams
Fibrous metals
Springs

ABSTRACT

Entangled structures, such as steel wool, can be used as inexpensive, high cycle, low stiffness, thin profile compressive springs where uniform pressure on a surface is required particularly in elevated temperature and/or harsh environments. Mechanical compression tests were performed on a variety of steel wool samples to determine the stress–strain curve behavior over high cycles. After initial conditioning cycles, good repeatability can be obtained with hysteresis dependent on strain. The results show a nonlinear behavior over large strains (>10%) and reasonable linear behavior for strains less than 10%. The properties of an entangled structure spring can be selected to achieve the desired stiffness for a particular application.

1. Introduction

The mechanics of a random array of interwoven fibers, i.e. entangled wires such as found in steel wool, have been studied for applications such as damping, isolating, or filtering. In semiconductor test applications "Fuzz Buttons," a compacted random array of wire, have been used as temporary electrical contacts for "low signal distortion, high frequency, and low insertion force, planarity, and shock/vibration resistance" [1]. Contact testers made from micro entangled structures have been used by the semi-conductor industry to test Through Silicon Via (TSV) and micro-bumps arrays [2,3]. The characterization of entangled wires is also very important for micro-electronics, micro fluidics, micro sensors and actuators that are based on entangled silica nano-wire structures [4]. The generation of the silica nanowire entangled arrays are grown, and not created via a mechanical means and they often appear as entangled [4,5]. Entangled structures are also used by the space industry to isolate instruments or to damp vibrations [6,7].

Entangled structures have also been evaluated as compatible replacements for porous aluminum as they have been shown to have good toughness and strength [8,9]. Entangled titanium wire materials (ETWM) and porous titanium foams have been considered for tissue reconstruction, orthopedic implants, and bone repairs [10–14]. The challenge for the medical industry has been to match the mechanical properties of entangled wire structures to similar mechanical properties of bone which has been attempted by altering the effective porosity of the structure created by the entangled wires [11,14]. While compressive properties and pseudo-elastic hysteresis behaviors have been characterized for ETWMs, a high cycle analysis of the nonlinear elastic region of ETWMs is needed to make the design process more deterministic.

Prior work has shown that entangled structures have a three-stage stress–strain behavior under compressive loads: (1) nonlinear elastic deformation, (2) strain-hardening, and (3) densifying [10]. Here we build on this work by studying the higher cycle compliance of entangled structures under uniaxial compression for the use as an inexpensive and repeatable low-moderate stiffness thin profile large contact area spring. This type of spring has wide application in presses and rectilinear format batteries. This work also examines the effect of densification on the apparent Young's modulus for entangled structures for comparison with existing analytical models. Analogies are made with low density materials such as foams, composites, and elastomers in order to help develop modeling tools.

2. Experimental procedures

2.1. Sample characterization

One method for generating an entangled metal wire structure involves wrapping the wire around a rod to create a loose steel wire bundle. The unconsolidated deformed wire is placed into a set of molds where it is compressed and sintered to remove internal stresses [8,10,15]. Common steel wool, which is much more compliant and inexpensive, is made by shaving small strands from straight steel wire and consolidating the strands into an entangled structure using a needle punch machine to generate a mat of wool. The

* Corresponding author. Tel.: +1 603 513 8997; fax: +1 603 225 3102.
E-mail address: Folkers.Rojas@gmail.com (F.E. Rojas).

http://dx.doi.org/10.1016/j.precisioneng.2015.04.013
0141-6359/

Table 1
Characterization of samples tested.

	For cyclic study	For densification and cyclic study
Initial size (mm^3)	$52 \times 52 \times 8.5$	$61 \times 63 \times 36$
Mass (g)	5.83	6.14

pads are held together by the entangling nature of the process that produces a semi-aligned structure with the fibers in the pad.[1] Prior work on characterizing steel wool pads was done in 2006 by Masse et al.; however, only 60 cycles were used to derive the stress–strain curve [16]. Their work showed that the stress–density curves had a power-law relation [16]. In the present work, we are interested in the cyclic performance of steel wool as a spring that acts over a wide area subject to thousands of cycles. Applications include providing a uniform pressure over the surface of an object as might be needed in a press or a rectilinear format battery.

To study high cycle behavior, two types of samples were initially evaluated: coarse (Grade #3) and fine (Grade #0) steel wool with wire diameters of 90 μm and 25 μm respectively were used. Test samples were cut from non-sintered steel wool pads.[2] The manufacturing method of the wool pad creates an inherent preferred orientation of a planar cross pattern.

Hydrostatic weighting is typically used for determining the porosity of a sample [10], in this case the mass of the sample was measured using an AG204 Delta Range Mettler Toledo scale with an accuracy of 0.1 mg/1 mg, at room temperature. The volume of a sample was measured with calipers accounting for an error of about 1 mm on each length measurement. The samples were cut from 7-in. diameter pads into squares as summarized in Table 1.

The objective of the densification experiment was to explore the repeatability over a range of compression states to determine effect of density on stiffness. The densification study is done with a highly porous steel wool sample (Grade 1 – purchased as a 1 pound bag from McMaster-Carr[3]) that is incrementally compressed while testing long term cyclic behavior at each stage. The sample used for the densification experiment does not contain the planar cross pattern of the wool pads. The sample is incrementally compressed until more than fifty percent strain has been achieved. At each state the sample is not strained more than ten percent at any given time.

2.2. Testing procedure

The stress–strain behavior of the samples was performed using an Admet testing machine (Model 5601QP2 – Serial 0611091 eXpert) with an Interference load cell, rated to 120 N (Serial # 708336). As shown in Fig. 1, the experimental setup consists of a base support with a pocket region for the samples that prevents horizontal shifting of the sample during the cycling process. A compressive plate provides an even load, measured by the load cell, across the sample. The testing machine is controlled by a programmed displacement cycle.

2.3. Cyclic testing

The preliminary tests, shown in Fig. 2, show the loading for a fine and course sample with ~97.7% porosity. The fine steel wool sample has a stiffer stress–strain response compared to the coarse sample, due to the limitation of the strain gauge only the course sample is tested extensively over a wider range of strains. The tests show a settling/shifting effect in the stress–strain curve over first 100 cycles in the non-linear elastic region. Van Wyk alluded to this shifting effect in his 1964 paper: "the curve shifts with each successive cycle of compression and release, but finally attains a steady position" [17]. After the initial settling the data was repeatable. The discrepancy is attributed to the initial settling and distortion of the entangled structure in the process toward reaching stability. A 1000 cycle run was thus used to remove any long term settling of the samples. As a check, a low stiffness coil spring was substituted for the sample to ensure that testing machine was operating as expected, and the result confirmed the observation of the entangled structure behavior.

The coarse sample was cycled on the testing machine at a frequency of 0.5 Hz and at a constant strain rate of 24%, 2 mm/sec over a sample height of 8.5 mm. The fine sample was also cycled at a 0.5 Hz, but with a smaller strain rate as the stiffness was higher than the coarse sample. The densification sample was also tested at a constant strain rate with sample thickness starting from 36 mm and decreasing to 22 mm by 2 mm increments. For the initial data set the steel wool is cycled from 36 mm down to 34 mm. The first thousand cycles are discarded from the data, to establish the steady state behavior. An additional two thousand cycles are performed and used to analyze the steady state behavior in that region. With the completion of the initial data set, the following data set starts from a 34 mm thickness and is cycled down to 32 mm. The same process is carried out to all following data sets until reaching a final thickness of 22 mm.

3. Results

The data collected from the testing machine is shown in terms of vertical displacement and the compressive load measured by the load cell gauge. The data is combined with the geometry and sample properties to generate engineering stress–strain curves, as shown in Fig. 3.

3.1. Cyclic testing

The coarse sample was loaded for >11k cycles, with an initial 1k cycle break-in period for allowing the fibers to settle into a steady state region. Note that this type of break-in period is also required for steel cables [18]. As shown in Fig. 4, every two thousand samples, the loading curve is repeatable and below the initial curve of the break-in period. The first 1k sample (i.e. break in) was where it reaches steady state. Then the system was set to do a 2k run, when done the same preload was affirmed and then a run was done for the next 2k sample (i.e. sample 2001 is the first value). Notice that the break in curve is higher than all of the other curves. Each data set following the break in consists of 2000 cycles. At the conclusion of each data set the sample is reset to the starting preload in the event that drifting in the testing machine took place during cycling. Only the first data point of each data set is plotted to illustrate repeatability. After collecting 11k cycles, the average of all the first data sets was calculated and plotted. Future work will calculate the mean and error of all of the data points combined.

3.2. Young's modulus as densification

The sample used for the densification is a homogeneous unconsolidated coarse steel wire wool with a diameter of 90 μm. The goal was to demonstrate that a small change in the porosity of the structure can result in a change in the effective stiffness. The cycle stroke was set to 2 mm, which limited the strain from 5.5% (at 36 mm) to 9.1% (at 22 mm), to the authors surprise the stiffness was linear in these regions. Fig. 5 shows the response starting from a 36 mm thick sample undergoing a minimum of 3000 cycle test, for clarity

[1] See for example http://www.youtube.com/watch?v=iaDzLP3TT_I.
[2] Manufacturer of Wool pads: International Steel Wool Inc. (http://steelwooldirect.com/) for the 7 inch Tex-Wool floor pads grade 0 and 3.
[3] Grade 1 Steel wool – 1 pound bag from McMaster-Carr Item Number 7363T24.

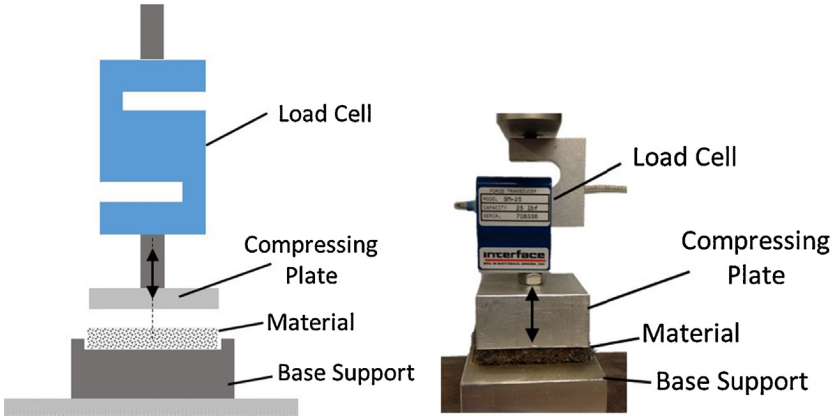

Fig. 1. System used to measure the cyclic stress–strain relation of the samples.

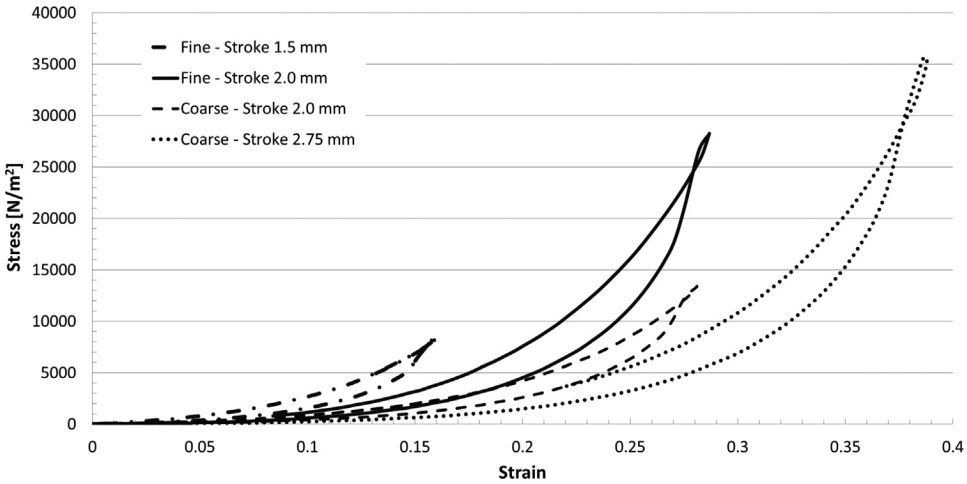

Fig. 2. Coarse versus fine characterization. Height of fine sample is 13.7 mm and coarse sample 14.0 mm. The data shown is for a complete cycle of load/unload. The stroke refers to the compression of the sample.

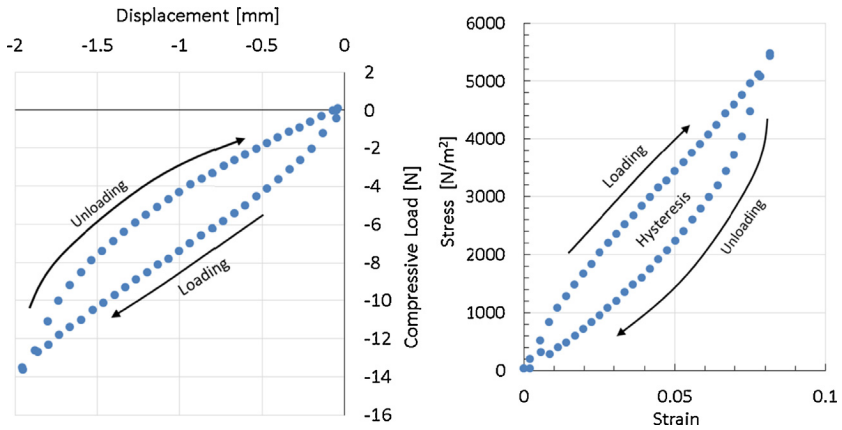

Fig. 3. Typical loading and unloading data from the tester and engineering stress–strain representation for the course sample.

only the loading portion of the graph is shown. The curves shown in Fig. 5 are the final sample of the compression test.

The nonlinear section in the initial one percent strain region is attributed to overcoming static friction between the fibers. It is hypothesized that as the strands begin to move pass each other, and friction transitions from static to dynamic, they achieve a steady state stiffness as observed. Fig. 6 illustrates how the preloaded samples stack and the effective stiffness is obtained as a function of the strain at each sample thickness.

4. Discussion

4.1. Models

There are four predominant models used to predict the mechanical behavior of entangled or porous structures: (1) Gibson–Ashby model, (2) Nielson model, (3) Baudequin relation, and (4) van Wyk model. Other prior work includes using finite element models to directly simulate the deformation of “dry” fiber networks, where

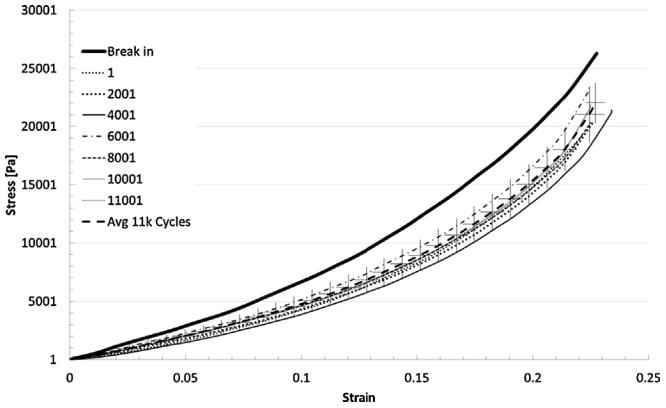

Fig. 4. Coarse steel wool sample loading behavior with initial thickness 8.5 mm and cyclically compressed to thickness 6.5 mm, and loaded at 2 mm/sec at a cycle frequency of 0.5 Hz. For clarity the data shown is for the loading portion of the test. The average is calculated taking the first sample of every thousand data set. The cross bars on the average line represent a standard deviation.

strands are assumed to be bonded together with elastic springs and no subsequent sliding takes place [19]. As shown by Rubshtein et al, the predicted Young's modulus can differ for the varying models [12]. Thus, the models are compared below for varying parameters, which will later be compared to the experimental data to establish applicability for the entangled structures tested herein.

The Gibson–Ashby equation is used to affirm that the applied stress is lower than the collapse stress of the entangled structure, where it is recognized here that this is an approximation since the Gibson–Ashby equation is for porous structures [20]; however, the Gibson–Ashby equation [20] can also be used to calculate the Young's modulus as well as the Yield strength for entangled media [8]:

$$\frac{\sigma^*_{pl}}{\sigma_{ys}} = C_1 \cdot \left(\frac{\rho^*}{\rho_s}\right)^{n_1} \tag{1}$$

$$\frac{E^*_{pl}}{E_{ys}} = C_2 \cdot \left(\frac{\rho^*}{\rho_s}\right)^{n_2} \tag{2}$$

where $\sigma^*_{pl}/\sigma_{ys}$ is the ratio of the plastic collapse stress of the porous material to the solid material yield stress, ρ^*/ρ_s is the ratio of the sample density to the solid density, and E^*_{pl}/E_{ys} is the elastic Young's modulus ratio of the porous structure to that of a solid. The values C_1, C_2, n_1, and n_2 are constants related to the porous structure. C_1 is typically about equal to 0.3 and n_1 is approximately 1.5 for a variety of foams [21]. Note that the constants are empirically determined.

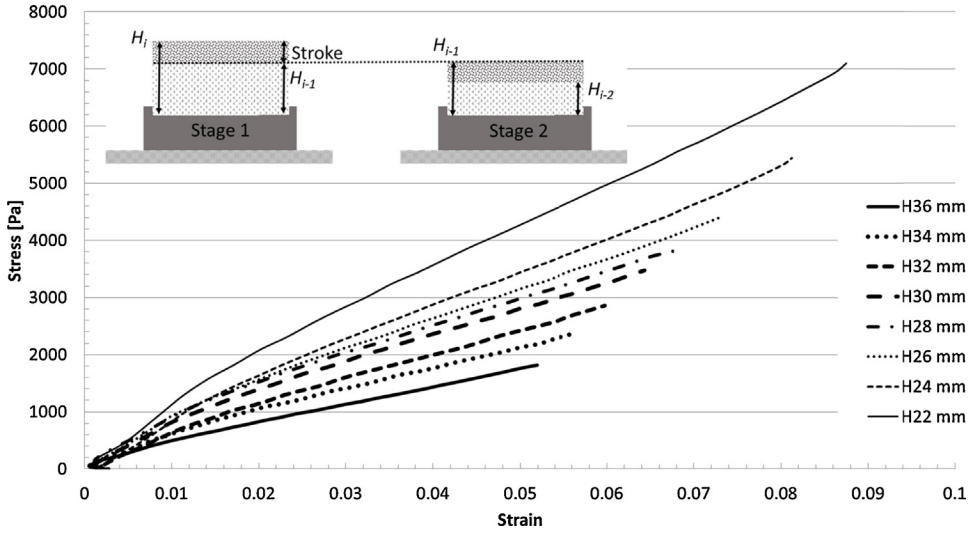

Fig. 5. Densification structure stress–strain curve of the loading section at each height.

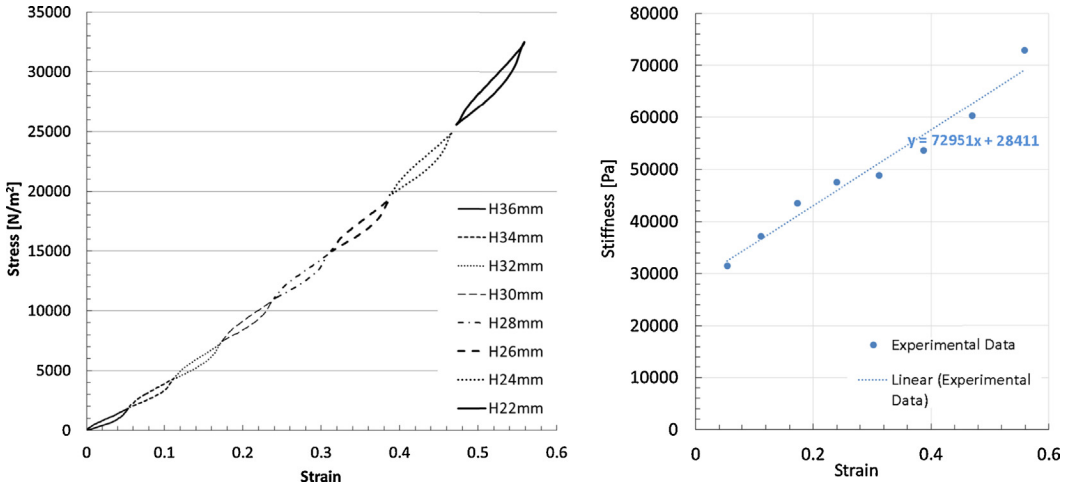

Fig. 6. (L) Stacked cycling response for densification sample. (R) Stiffness measured for the array of strain densification tests.

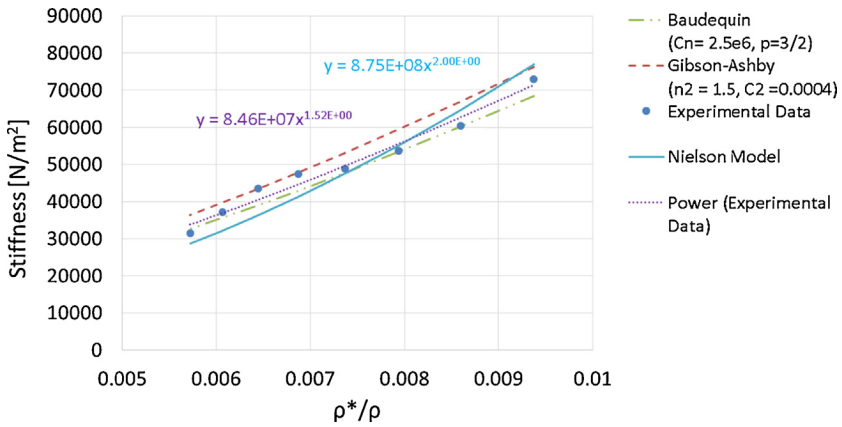

Fig. 7. Analytical model comparison between experimental data and analytical model.

The Nielsen model has also been used to calculate the expected Young's modulus for a porous elastic material as a function of porosity [22].

$$E^* = E_s \cdot \frac{(1-\theta)^2}{1+(1/\varphi-1)\varphi} \tag{3}$$

where θ is the porosity, and ϕ is a geometric factor as a function of area and perimeter

$$\varphi = \frac{4 \cdot \pi \cdot Area}{P^2} \tag{4}$$

The Baudequin power law relation for glass wool, where the stress is proportional to the strain to the $-3/2$ power, has been supported by experimental data [23]. Since the material properties of glass wool are different than those of steel wool, the relation may not be applicable but only experimental data will tell.

$$\sigma \propto (\varepsilon^* - \varepsilon)^{-3/2} \tag{5}$$

The van Wyk model consists of relating the global behavior of the sample to beam bending dynamics at the micro scale [17]. The derivation is similar to the work done by van Wyk and Pawlak et al. [17,24]. Eq. (6) is the basic equation used for the Wyk derivation.

$$dF = \frac{k \cdot Y \cdot I_c}{S^3} \cdot dy \tag{6}$$

where k is an unknown factor due to the variability in the geometry of contact and that the points of contact are not regularly spaced, S is the mean distance between the fibers. The resulting equation (7) is used to correlate the "resistance to compression" (i.e. Stiffness) to physical values:

$$A = \frac{\alpha \cdot Y \cdot m^3}{\rho^3} \tag{7}$$

where α is a constant (to be found experimentally), m is the mass, and ρ is the density of the wool.

A comparison of the models to the experimental data shows that the Gibson–Ashby model best matches the data collected. While the trend of the Nielson model shows that with increasing porosity the stiffness decreases, the model over estimates the expected Young's modulus by at least by two orders of magnitude; the effect of the geometric area is not significant enough to compensate for the discrepancy. The Nielson model has a trend to the second power, which does not match the data accurately. Baudequin et al.'s relation, derived for glass wool, between compressive stress and how it is related to the strain to a $-3/2$ power did not match the measured our data [23]. The observed behavior has the strain to a positive 3/2 power, which matched the data. The trend predicted by the van Wyk model does not match the data.

As shown in Fig. 7 the Gibson–Ashby model, with $n_2 = 1.5$ and $c_2 = 4e{-}4$, reasonably predicts the stiffness observed from the densification samples. The Nielsen model yields a higher Young's modulus of the materials without capturing the nonlinear behavior. The Baudequin model has an inverse stiffness–strain relation to that observed in the data, and as the strain increases the models predict a drop in the stiffness. As shown in Fig. 8, the percentage error of the models ranges between about ±15%.

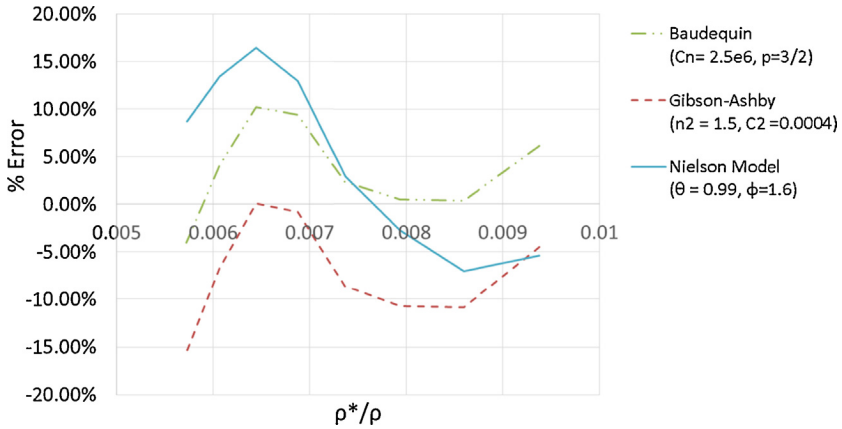

Fig. 8. Percentage error of analytical models.

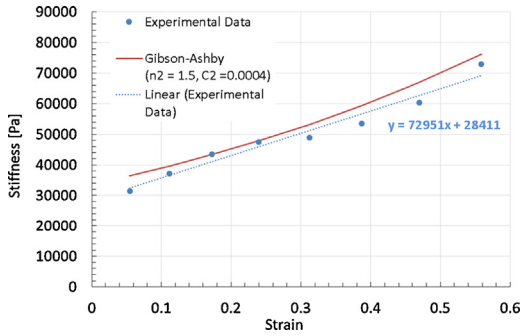

Fig. 9. Strain versus stiffness behavior for the densification experiment with an overlay of the Gibson–Ashby model.

4.2. Elastic hysteresis

The separation between the loading and unloading curves that allude to hysteresis, a known characteristic of entangled structures, is attributed to the friction between wire elements sliding across each other during loading. Another hypothesis is the non-linearity comes from contacts being created during the compression process [23]. The curved shape of the stress–strain curves indicates the complex mechanics that take place during the elastic stage, whereas the porosity decreases hysteresis is smaller. The findings confirmed the power-law relation of the stress–strain curve; however, it also showed an entry/break-in time period where the samples' properties change as the number of cycles increase. When repeatability is needed, the drifting that occurs upon initial use must be removed by cyclically loading (break-in period) the samples over 100 times prior to establish steady state behavior and then using them in a preloaded state. Although the friction/slip between the fibers is irreversible the long term cycle loading behavior appears reasonably repeatable, allowing for use as a constant force (pressure over a wide area), low-moderate stiffness spring.

4.3. Porosity dependence

Similar to tensile tests performed by others [10,15] the compressive properties of entangled structures strongly depend on the porosity of the sample, where larger porosity results in lower Young's modulus. Other research has examined entangled steel wire materials using stereomicroscopes and scanning electron microspores to gain insight into the tensile dynamics of an entangled structure [15]. The high cycle tests results collected herein showed that the complex intertwined structure has modest hysteresis and thus can be used as a spring especially when the strain about any particular preload is kept less than ±10%.

4.4. Densification

Preloading the samples (densification) to a fixed thickness and then cycling them by a fixed amount about the preloaded thickness revealed a linear region for highly porous structures where the stiffness was constant and repeatable and can be characterized as a function of porosity. Thus it is foreseeable to vary preload, geometry, and materials to acquire a desired linear stiffness for highly porous materials used as springs acting over a wide area (Fig. 9).

5. Conclusion

The high cycling of entangled structures about a set preloaded thickness has been demonstrated to show their potential use as a thin low stiffness spring acting over a wide area. It was also shown that highly porous structures can exhibit linear stiffness for low strains. One advantage of this material is its ability to conform to an irregular surface while still allowing for the mechanical properties to be altered by changing the porosity. Hence entangled structures can be used as an alternative to foam pads for applying pressure to an object. In particular, at elevated temperatures or in aggressive environments, stainless steel wool has particular promise as a thin profile area spring.

References

[1] Custom interconnects – fuzz button performance; 2014. Available from: http://www.custominterconnects.com/ (23.06.14).
[2] Yaglioglu O, Eldridge B. Direct connection and testing of TSV and microbump devices using nanopierce contactor for 3D-IC integration. In: 30th IEEE VLSI test symposium. 2012.
[3] Yaglioglu O [Doctor of Philosophy] Carbon nanotube based electromechanical probes. Mechanical Engineering Massachusetts Institute of Technology; 2007.
[4] Woldegiorgis A, Jansson K, Roerrade J. Fabrication of silica nano wires on the internal perimeter of narrow bore fused silica tubing by non-isothermal etching. J Mater Sci 2005:583–9.
[5] Yan C, Zhang T, Lee PS. Flow assisted synthesis of highly ordered silica nanowire arrays. Appl Phys A: Mater Sci Process 2009;94:763–6.
[6] Castagnede B, Moussatov A, Lafarge D, Saeid M. Low frequency in situ metrology of absorption and dispersion of sound absorbing porous materials based on high power ultrasonic non-linearly demodulated waves. Appl Acoust 2008;69:634–48.
[7] Sun F, Chen H, Wu J, Feng K. Sound absorbing characteristics of fibrous metal materials at high temperatures. Appl Acoust 2010;71:221–35.
[8] Tan Q, Liu P, Du C, Wu L, He G. Mechanical behaviors of quasi-ordered entangled aluminum alloy wire material. Mater Sci Eng A 2009;527:38–44.
[9] Tan Q, He G. 3D entangled wire reinforced metallic composites. Mater Sci Eng A 2012;546:233–8.
[10] Liu P, Tan Q, Wu L, He G. Compressive and pseudo-elastic hysteresis behavior of entangled titanium wire materials. Mater Sci Eng A 2010:3301–9.
[11] Barbas A, Bonnet AS, Lipinski P, Pesci R, Dubois G. Development and mechanical characterization of porous titanium bone substitutes. J Mech Behav Biomed Mater 2012:34–44.
[12] Rubshtein AP, Trakhtenberg IS, Makarova EB, Triphonova EB, Bliznets DG, Yakovenkova LI, Vladimirov AB. Porous material based on spongy titanium granules: structure, mechanical properties, and osseointegration. Mater Sci Eng C 2014:363–9.
[13] Chen YJ, Feng B, Zhu YP, Weng J, Wang JX, Lu X. Fabrication of porous titanium implants with biomechanical compatibility. Mater Lett 2009:2659–61.
[14] Krishna BV, Bose S, Bandyopadhyay A. Low stiffness porous Ti structures for load bearing implants. Acta Biomater 2007;3:997–1006.
[15] Liu P, He G, Wu L. Uniaxial tensile stress–strain behavior of entangled steel wire material. Mater Sci Eng A 2009;509:69–75.
[16] Masse JP, Salvo L, Rodney D, Brechet Y, Bouaziz O. Influence of relative density on the architecture and mechanical behaviour of a steel metallic wool. Scr Mater 2006;54:1379–83.
[17] Wyk CM v. Note on the compressibility of wool. J Text Inst 1946:T285–92.
[18] Werkmeister JB, Slocum AH. Theoretical and experimental determination of capstan drive stiffness. J Int Soc Precis Eng Nanotechnol 2007 January;31:55–67.
[19] Kulachenko A, Uesaka T. Direct simulation of fiber network deformation and failure. Mech Mater 2012:1–14.
[20] Gibson LJ, Ashby MF. The mechanics of three-dimensional cellular materials. Proc R Soc Lond Ser A 1982:43–59.
[21] He G, Liu P, Tan Q. Porous titanium materials with entangled wire structure for load-bearing biomedical applications. J Mech Behav Biomed Mater 2012:16–31.
[22] Nielsen LF. Elasticity and damping of porous materials and impregnated materials. J Am Ceram Soc 1984;67:93–8.
[23] Baudequin M. Non-linear elastic behavior of light fibrous materials. Eur Phys J B 1999;12:157–62.
[24] Pawlak JJ, Keller DS. The compressive response of a stratified fibrous structure. Mech Mater 2005;37:1132–42.